



Atomic and microstructural origin of banded colours in purple-blue variety of agate from Yozgat Province, Turkey

Roberto Lorenzi¹ · Andrea Zullino² · Valentina Gagliardi² · Loredana Prosperi² · Alberto Paleari¹ · Ilaria Adamo²

Received: 6 April 2022 / Accepted: 27 June 2022
© The Author(s) 2022

Abstract

Agates from Yozgat province are appreciated on the gem market for their white and purple-blue banded colours. In this study, we present a detailed investigation aimed at the identification of the atomic and structural origin of this peculiar colouration of chalcedony. X-ray diffraction and Raman spectroscopy revealed the presence of fine grains of quartz and moganite with a preferential accumulation of the latter in the blue bands. Near-infrared diffuse absorption spectra show overtones of hydroxyls vibrations at 1425, 1900, and 2250 nm. In the visible, the broad absorption at about 500 nm, as well as its behaviour at low temperatures, is compatible with the optical activity of iron impurities in quartz matrices, such as that observed in amethysts. Peak intensities and shapes are very similar for spectra collected in blue and white bands. Accordingly, trace-element composition from laser ablation inductively coupled mass spectrometry confirmed that the two regions have similar Fe content. The perceived changes in band colours are indeed originated by differences in microstructural arrangement and size of the grains visualised through scanning electron microscopy. White and blue stripes have grains of about 5 µm and 300 nm in size, respectively, resulting in an accentuated scattering component for the white bands. Therefore, the unique purple-blue shades typical of Yozgat agates are a combination of iron-related colour centres and scattering effect.

Keywords Agate · Chalcedony · SEM · Raman · Absorption · Iron

Introduction

Chalcedony is a micro- or crypto-polycrystalline form of silica which has the chemical formula SiO_2 . It comes in a wide variety of patterns and colours (Gliozzo 2019). Many of these varieties have specific names, such as the green chrysoprase, orange-red carnelian, bloodstone, onyx, and agate, which, in particular, is the variety that displays a distinct banding with successive different coloured layers (O'Donoghue 2006). The different varieties of chalcedony, including agate, have been used for a long time as gemstones in jewellery and as carving materials for producing ornamental objects, such as cameos and intaglios. The typical silica phases occurring in chalcedony are α -quartz, the most relevant mineralogical phase, and moganite, a polymorph

of silica, approved as a new mineral species in 1999 by the Commission on New Minerals and Mineral Names of the International Mineralogical Association (Heaney et al. 2007). Moganite has a widespread distribution in most microcrystalline SiO_2 varieties (Heaney and Post 1992) and, in particular, is commonly inter-grown with quartz in chalcedony. Moganite has a monoclinic symmetry, instead of the trigonal symmetry of α -quartz and its structure consists of alternating (101) layers of right- and left-handed α -quartz, twinned periodically at the unit-cell scale according to the Brazil-law (Miehe and Graetsch 1992). Agate occurs in a wide range of colours, which are caused by a variety of different impurities, occurring as trace elements substituting Si or as embedded minerals (Götze et al. 2001). According to Götze et al. (2001), iron oxides are the main colouring pigments in orange- and red-coloured agates. The characteristic rhythmic colour banding seems to be largely chemically controlled, reflecting variations in the deposition of pigmenting impurities. The origin of colour, in particular the blue one, can also result from light scattering, but the exact causes of this optical phenomenon in agates are still unclear and strongly depends on the geological specificity of

✉ Roberto Lorenzi
roberto.lorenzi@unimib.it

¹ Department of Materials Science, University of Milano-Bicocca, Via Cozzi 55, 20125 Milan, Italy

² Istituto Gemmologico Italiano (IGI), Piazza San Sepolcro 1, 20123 Milan, Italy

the extraction site. According to Zolensky et al. (1988) and references therein, blue colouration is believed to arise by Rayleigh scattering from submicrometric-sized solid mineral inclusions, whereas in Deer et al. (2004), the bluish-grey colour is attributed to scattering of light from fine-grained chalcedony fibres. Chalcedony, including agate, can be found in deposits all over the world, in widespread geological environments. For many centuries, Turkey has been known for being an important source of multi coloured, gem-quality chalcedony. There are many blue chalcedony deposits with economic reserves located in different regions of Turkey. According to Hatipoğlu and Chamberlain (2009) and Hatipoğlu et al. (2013), they include: Saricakaya (Eskisehir), the most relevant Turkish blue chalcedony deposit used since the Roman period, Kibriscik (Bolu), Bayat (Afyon), Aliaga and Bergama (Izmir), and Zile (Tokat). Recently, purple-blue agates coming from the Yozgat Province, which is located in the northeast part of central Anatolia, have come onto the gem market (Başbüyük 2018). The agate samples from the Yozgat area can be found in the cavities of post-Lutetian alkaline andesites volcanic host rocks (Büyükonak 1985). The formation of this agate, accompanied by presence of amethyst, white quartz, and reddish brown amethyst (Başbüyük 2018), occurred during secondary processes in volcanic rocks, which is the most common process of agate genesis (Götze et al. 2001). In this work, we present a characterisation of agate from Yozgat Province, investigating both the bulk mineralogical composition by means of X-ray powder diffraction and the mineralogical phases' variations in correspondence of the differently coloured bands using confocal micro-Raman spectroscopy. The aim of this study is to provide an explanation of the origin of banded colours of Turkey purple-blue agate by combining XRD and Raman investigation with trace-element composition analysis, UV–Vis–NIR spectroscopy, and scanning electron microscopy.

Materials and methods

Minerals and gemmological tests

In the present study, we have examined agates from Yozgat, the sample set includes one rough sample (76 g), one cabochon cut gems (1.95 ct), and a 1 mm thick polished slab. The gemmological properties were measured only on cabochon cut specimen. The refractive index was measured using a Kruss refractometer with ordinary light source with a sodium filter (589 nm) and methylene iodide saturated with sulphur as a contact liquid (RI = 1.80). A Mettler hydrostatic balance was used to determine the specific gravity in distilled water, whereas the ultraviolet fluorescence was

investigated with a short (254 nm) and long (366 nm) wavelength ultraviolet Analytic Jena Wood lamp.

Phases' identification

X-ray powder diffraction (XRD) measurement were carried out on the rough sample, previously crushed, by means of a PANanalytical X'Pert Pro diffractometer, equipped with an X'Celerator detector, using CuK α radiation. A step scan of 0.02° 2 θ was performed over the range 15–80° 2 θ . Confocal Raman microscopy has been performed with a Labram (JobinYvon) spectrometer and a He–Ne laser at 632.8 nm, focussing the beam on a circular spot of about 2 μ m through the optics of a microscope (Olympus) and a long working distance objective with magnification 50 \times and NA 0.60. The diffused light was detected in backscattering configuration by means of a Peltier-cooled silicon charge-coupled-device detector, after a notch filter and a monochromator with a spectral resolution of 1 cm⁻¹.

Chemistry determination

Quantitative elemental analysis was performed by Laser Ablation Inductively Coupled Mass Spectrometry (LA-ICP-MS), using an ICP-MS PerkinElmer ELAN DRC-e coupled to a sampler New Wave UP 213 working with a quintupled Tempest laser at 213 nm. The protocol used for this analysis is based on the PerkinElmer proprietary semiquantitative method TOTALQUANT based on the instrument internal standardisation. For this analysis, the internal standardisation has been improved by a single measure of NIST SRM 610, a glassy multielemental solid standard.

UV–Vis spectroscopy

Optical absorption spectra were measured using a Perkin Elmer Lambda 950 spectrophotometer equipped either with a standard Photomultiplier detector or with a 60 mm Spectralon-coated integrating sphere. In-line transmission spectra were recorded placing the sample in the optical focus of the spectrophotometer at about 10 cm from the entrance port of the standard detector, whereas diffuse absorption was measured positioning the sample at the entrance port of the integrating sphere. Low-temperature spectrum was collected with in-line geometry and using a GALILEO cryocooler.

Electron microscopy

Morphologies were analysed by scanning electron microscopy (SEM; Tescan Vega Model 5136XM). Before image acquisition, samples underwent to chemical etching using a 10% vol solution of hydrofluoric acid (Sigma Aldrich) in deionized water for 5 min. Finally, samples were coated with

a thin film (about 10 nm) of gold using a sputter coater Quorum Q150RS.

Results and discussion

Sample description, crystallographic phases, and composition

The chalcedony samples from Yozgat are all translucent with a pale purple-blue colour, distributed in bands of millimetric size, photographs of the rough sample and of a polished slab are reported in Fig. 1. The refractive index measured at 589 nm by the distant vision method is 1.53, whereas the density ranges from 2.56 to 2.59 g/cm³. These values are consistent with data reported in the literature on cryptocrystalline quartz minerals (O'Donoghue 2006). The samples exhibit a weak to moderate bluish white reactions to both long- and short-wave UV radiation, without evidence of strong luminescence phenomena.

The XRD pattern of the powdered sample (Fig. 2), representative of both blue and white bands, presents peaks ascribable to silica polymorphs, specifically quartz and moganite. The strongest peaks located at 20.9° and 26.7°

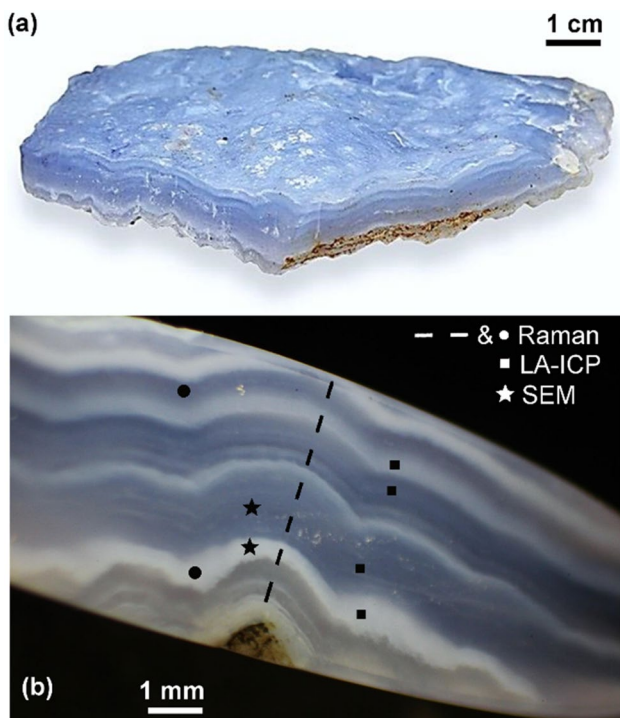


Fig. 1 **a** Photograph of the rough sample of agate from Yozgat, Turkey and **b** reflected light microscopy image of a plane and parallel cut slab sample about 1 mm thick. Indicative location of Raman measurements (dots) and line mapping (dashed line), LA-ICP (squares), and SEM analysis (stars) are reported

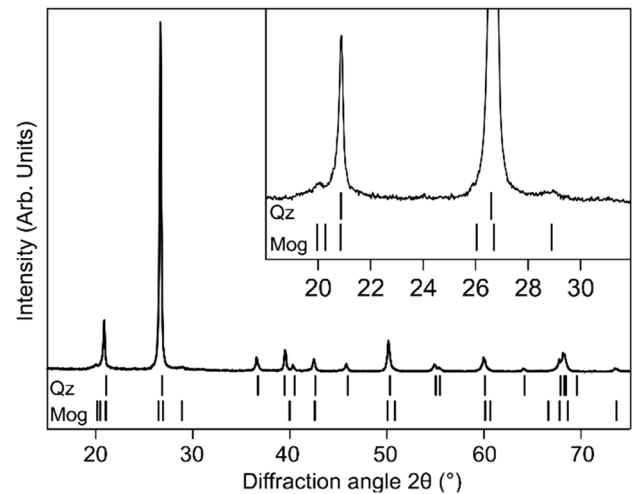


Fig. 2 X-ray diffraction of powdered sample, expected position of the main diffraction peaks of quartz and moganite are reported as line guides

correspond to diffraction from the (100) and (101) planes of α -quartz, respectively, accompanied by all the expected minor reflections (JCPDS card no. 46-1045). The presence of moganite is often masked by the diffraction pattern of quartz as a result of their high similarity (Graetsch et al. 1987; Smith 1998). However, characteristic signals from moganite can be found by analysing in detail the diffraction pattern in the range 18°–32° (Lee et al. 2021; Rodgers and Cressey 2001). Indeed, we register moganite reflections as minor contributions in this region (inset of Fig. 2). Shoulders at 19.9°, 25.9°, and 28.9° are ascribable to diffraction from (110), (−121), and (−112) planes of moganite, respectively (JCPDS card no. 38-360).

Another technique for the discrimination between quartz and moganite is Raman spectroscopy (Rodgers and Cressey 2001). In addition, in this case, there are strong overlaps between the two spectra as a consequence of the similarities in the crystal structures (Kingma and Hemley 1994). The differentiation is normally based on the position of the main Si–O–Si vibration which is located at 464 cm^{−1} and 501 cm^{−1} for α -quartz and moganite, respectively. Although the attribution of the 501 cm^{−1} band to Si–O–Si vibration in moganite is controversial and it is possibly related Si–O vibrations of non-bridging Si–OH (Schmidt et al. 2013, 2012).

The Raman spectrum of the sample effectively shows the presence of both phases (Fig. 3a). Acquiring spectra in correspondence of white and blue bands leads to very similar results. In both cases, the spectra are fully compatible with the reported data on α -quartz with main A₁ mode contributions at 206 cm^{−1} and 465 cm^{−1}, corresponding to Si and O displacement around the threefold screw axis and the symmetric bend of SiO₄ tetrahedra, respectively (Masso et al.

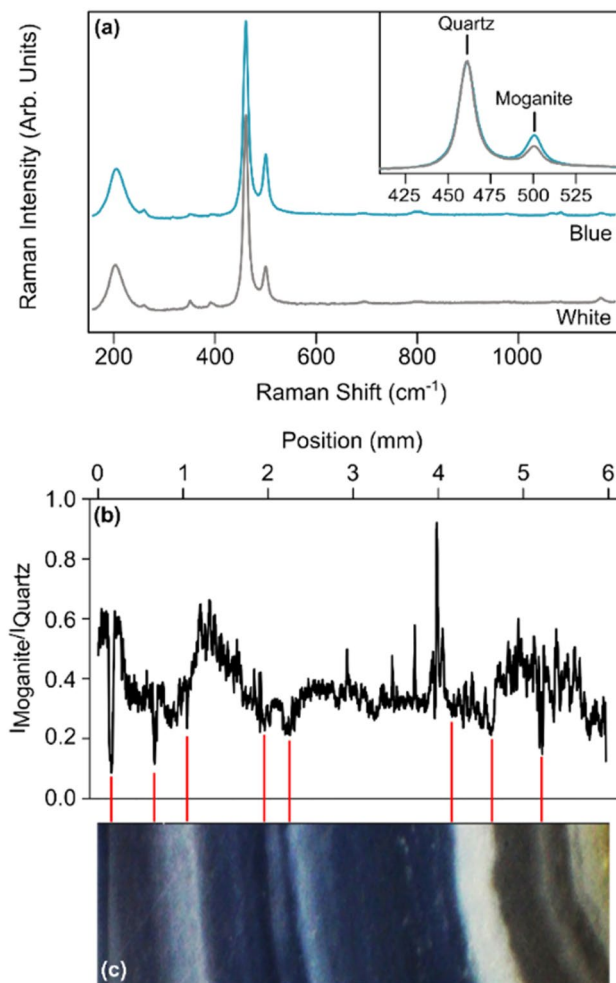


Fig. 3 **a** Raman spectra of a 1 mm thick slab collected on white and blue zones. **b** Raman line map of the intensity ratio of moganite/quartz signal taken perpendicularly to band alignment, the map corresponds to the sample photograph reported in **c**

1970; McMillan and Hess 1990; Umari et al. 2001). In addition, the characteristic peak of moganite at 501 cm^{-1} can be appreciated. Importantly, neither XRD nor Raman analyses register the presence of phases other than quartz and moganite. A more detailed comparison of Raman peaks in blue and white bands indicates that the relative abundance of the two phases is not constant across the sample. Spectra normalised to the quartz peak maximum indicate that bluish stripes have a more intense moganite peak with respect to white stripes (inset in Fig. 3a). We highlight that changes in the peak at 501 cm^{-1} may be originated also by different content of SiOH groups; however, we did not observe strong differences in hydroxyl content from near-infrared absorption features which will be discussed in detail further on. The same behaviour has been observed in other agates found in Permian basalt rocks showing moganite accumulation in the darker regions (Dumańska-Słowik et al. 2018). Further

Table 1 Results of the main ions measured by LA-ICP analysis for white and blue bands and their difference

Element	Content (ppm)		
	White	Blue	Difference (white–blue)
Li	20 ± 5	15 ± 4	$+5 \pm 8$
Na	156 ± 12	141.7 ± 0.4	$+14 \pm 12$
Mg	9.4 ± 1.6	7.2 ± 0.8	$+2 \pm 2$
Al	17 ± 4	13.3 ± 0.5	$+3 \pm 4$
K	63 ± 4	53 ± 3	$+10 \pm 8$
Sc	2.14 ± 0.11	1.69 ± 0.03	$+0.40 \pm 0.14$
Ti	3.5 ± 0.4	3.4 ± 0.9	0.0 ± 1.4
Fe	19.5 ± 1.1	23 ± 4	-3 ± 5
Cu	3.6 ± 1.1	2.78 ± 0.16	$+0.8 \pm 1.3$
Zn	2.31 ± 0.16	2.52 ± 0.08	-0.2 ± 0.2
Ge	9 ± 3	21 ± 4	-12 ± 8
As	4.7 ± 0.1	4.8 ± 0.1	-0.1 ± 0.2
Zr	108 ± 24	141 ± 4	-33 ± 28
Hf	2.4 ± 0.5	2.2 ± 0.4	0.2 ± 0.9
Ta	1.42 ± 0.09	1.11 ± 0.02	0.32 ± 0.11

information on the relation between moganite content and agate bands comes from Raman map analysis along a line perpendicular to agate bands. After baseline removal, the intensity ratio of moganite (501 cm^{-1}) over quartz peaks (465 cm^{-1}) has been studied as a function of the position along the line collecting a spectrum every $2\text{ }\mu\text{m}$. The line map (Fig. 3b) confirms that the ratio follows a trend related to the bands. In particular, an accumulation of quartz can be noted in correspondence of boundaries between bands (red lines in Fig. 3b and c). This is the result of the peculiar accretion of agates which leads to preferential formation of different structures or accumulation of impurities at the edges of the bands (Park et al. 2015; Walger et al. 2009). The intensity ratio, excluding local maxima and minima, varies between $\approx 20\%$ and 60% . This range corresponds to a moganite content of the order of $50\text{--}75\text{ wt}\%$ (Götze et al. 1998). It is well known that moganite content in agates is a good indicator of the forming era (Moxon and Ríos 2004), and our results are in good agreement for agates found in volcanic rocks formed in Eocene period (Zhang et al. 2020). Remarkably, this change of phases across bands is not associated with strong differences in the chemical composition of the bands. Table 1 summarises the average value of the concentrations of trace elements measured by LA-ICP-MS and collected in four different points on white and blue bands. The results are qualitatively in accordance with those reported by Başbüyük (2018) from agate mined in the same region, albeit our concentration is one order of magnitude lower. It is interesting to note that the small but statistically significant variations between the white and blue areas

concern only ions that do not cause significant colouration in quartz. In fact, among all the elements identified, possible sources of greyish and bluish tints in the quartz can be traced back to Al, Ti, and Fe ions (Götze et al. 2021; Rossman 2018; Seifert et al. 2011). Moreover, although the iron content is quite low, it is high enough to induce violet colouration in amethyst quartz (Barry et al. 1965; Czaja et al. 2017; Dennen and Puckett 1972). Indeed, absorption spectra, reported in Fig. 4, reveal band possibly related to iron impurities. The in-line absorption is characterised by a strong tail which covers almost all the visible spectra, arising from Tyndall effect and Rayleigh scattering, typical of blue chalcidony (Götze et al. 2020). This scattering contribution gradually attenuates in the infrared, where hydroxyl overtones, either from SiOH and free water, can be easily detected at 1425, 1900, and 2250 nm (Flörke et al. 1982; Murphy 2015). Superimposed to the scattering tail a minor shoulder contribution can be distinguished at about 500 nm. This peak can be fully appreciated by taking the same spectrum in diffuse geometry. It is very broad, with a full width

at half maximum (FWHM) of more than 100 nm, and it is centred at 570 nm. Indeed these peak position and FWHM is compatible with one of the three peaks distinguishing the violet colour of amethyst (Rossman 2018). These three peaks are approximately located at 357, 545, and 950 nm and they are very sensitive to light polarisation and direction (Hassan and Cohen 1974). Their precise origin has been debated for long times, although the attribution is undoubtedly related to iron impurities. In particular, they are considered to arise from absorption of Fe^{4+} in tetrahedral coordination (Rossman 2018), possibly originated by precursors of Fe^{3+} and H^+ or other alkali metals (Di Benedetto et al. 2010). In addition, the position and relative intensity of these bands is the result of the thermal history of the amethyst covering. The 545 nm peak can shift up to 620 nm and, as a consequence, the same sample may appear coloured in purple, grey or yellowish only by changing the treatment temperature (Cheng and Guo 2020). Thus, the observed characteristics of the 570 nm peak in our sample is in agreement with Fe-related colour centres of amethysts and, notably, in some geodes from Yozgat Province this mineral has been found associated with agates (Başbüyük 2018). Further experimental evidence about this interpretation can be found examining the absorption peak collected at low temperature (inset of Fig. 4a), which basically remains unaltered with respect to room temperature measurement. The registered minor blue-shift and slight area increment is indeed in accordance with the behaviour reported in the literature (Bappu 1952). A last consideration about diffuse absorption features regards the acquired spectra collected in correspondence of blue and white stripes on a thick sample of about 5 mm with cabochon cut (Fig. 4b). It is evident that the two spectra are very similar and the small variations in intensity can be attributed to small differences in the local sample thicknesses. Importantly, this consideration implies two important consequences: (1) the hydroxyl content is very similar in the two regions, thus supporting the hypothesis that the differences observed in the intensities of the 501 cm^{-1} Raman line are mainly due to differences in the moganite/quartz ratio content rather than in Si–OH content and (2) that the apparent band coloration is not due to different concentration of colour centres since collecting the transmitted diffuse light there are no appreciable changes in the shape and strengths of absorption peaks. The change of colour is, therefore, controlled by some nano- or microstructural characteristic which dictates the diffuse to in-line transmission ratio and, eventually, the resulting band tints seen by the eyes. Effectively, the SEM images taken on white (Fig. 5a) and blue (Fig. 5b) bands show significant differences in crystallites mean size. The particle dimensions in the white zones are about $5\text{ }\mu\text{m}$, while in the blue ones is about 300 nm. If now we consider the scattering of a compact agglomeration of birefringent crystallites, then the

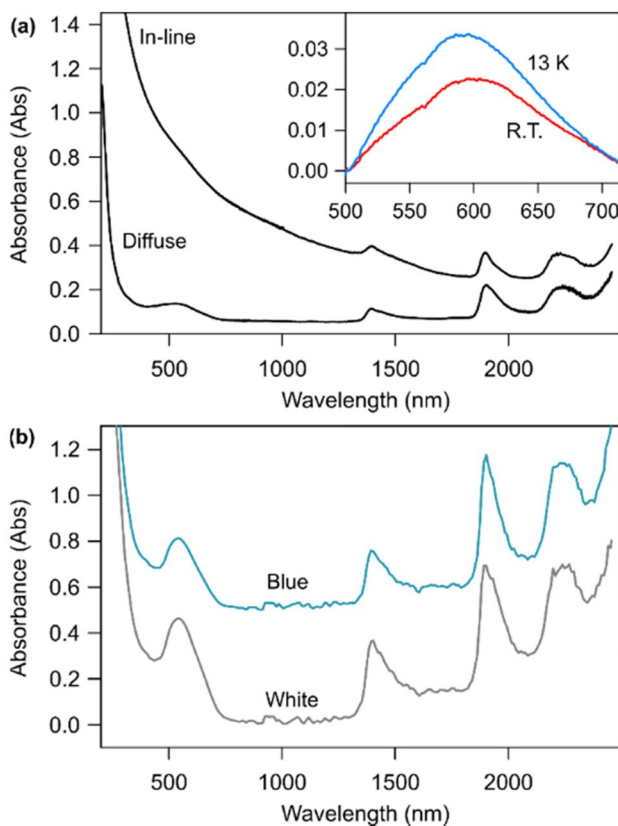


Fig. 4 **a** In-line and diffuse absorption spectra of a slab about 1 mm thick, spectra are collected on an area which covers both blue and white bands. Inset: main peak spectrum collected at room temperature and at low temperature. **b** Diffuse absorption spectra collected on a cabochon cut sample about 2–3 mm thick and collected in correspondence of blue and white bands

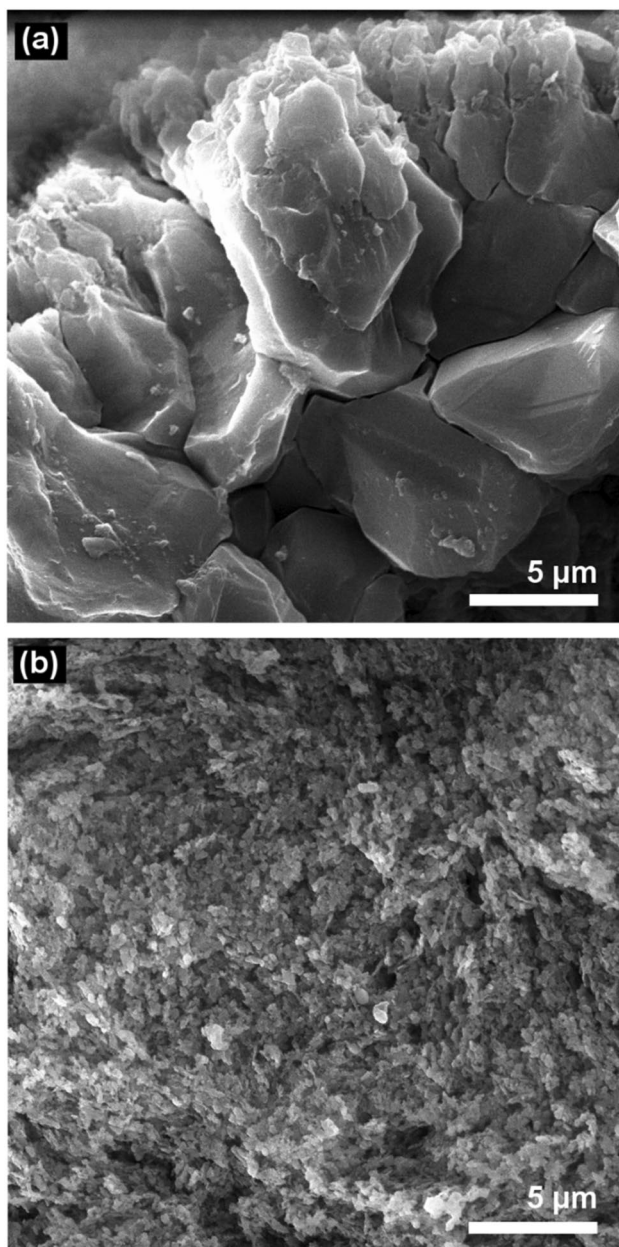


Fig. 5 SEM images at 10kX magnification collected on white **a** and blue **b** bands

expected in-line transmission is inversely proportional to grain size (Apetz and Van Bruggen 2003). The loss scattering contribution γ can be expressed as a function of wavelength λ , birefringence (with refractive index anisotropy Δn), and crystallite radius r as $\gamma = 3 \frac{\pi^2 \Delta n^2}{\lambda} r$ (Apetz and Van Bruggen 2003). If we neglect differences in refractive indices of quartz and moganite and we assume that the anisotropy Δn is equal for the two polymorphs, then the expected scattering losses for the white part will be about 16 times greater than those of the blue zone (i.e. it increases as the ratio of crystallites size). Since this is a Mie scattering, it

affects almost all the visible wavelengths and the appearance of bands with big grains will be milkier and opaquer. This also implies that the colour due to the peak at 570 nm will be emphasised where the scattering losses are lower since the scattering will play a minor role in these zones. It should be noted that in agate samples also the Rayleigh scattering plays an important role. In this case, the power law governing the scattering losses as a function of wavelength is of the form $\gamma \propto \lambda^{-4}$ (Naus and Ubachs 2000). Therefore, the blue part of the spectrum is more affected by scattering with respect to the green and red ones leading to a blue coloration. We can argue that, for this particular type of agates, the colour is the results of different contributions. In white bands, the Mie scattering is the dominant effect, while for blue bands, this effect is significantly reduced and the resulting colour is partly due to the presence of Fe ion impurities, as in amethysts, and partly due to Rayleigh scattering.

Conclusions

Using different experimental approaches, we have identified the main chemical, structural, spectroscopic, and morphological features of banded agates from Yozgat Province. Moganite content follows the rhythmic bands typical of agates with a preferential location in blue bands possibly accompanied by differences in hydroxyl content. The chemical composition between different bands is quite similar, especially as regard colour-bearing impurities. Both blue and white bands exhibit very similar diffuse absorption spectra, characterised by peak attributable to Fe impurities closely resembling those found in amethysts. The origin of different colouration between bands is indeed caused by structural features and not by strong differences in the volumic number of colour centres. White bands are in fact constituted by a compact matrix of crystallites of the order of few microns which causes strong Mie scattering. Purple blue bands are instead formed by tiny crystals of the order of few hundreds of nanometres. This structure has two main consequences on the apparent colour of blue bands: (i) the amethyst-like peak is enhanced when the agate is viewed in in-line transmission and (ii) the Rayleigh effect is also enhanced causing a further increase of blue shades. The combination of these two concomitant processes leads to the unusual purple-blue nuances distinctive of Yozgat agates.

Acknowledgements Financial support from University of Milano-Bicocca through grant ‘‘Bando Infrastrutture di Ricerca—Edizione 2021’’ is gratefully acknowledged. The authors gratefully thank Bülent Akdeniz for providing the samples, Dr. Monica Dapiaggi from the Department of Earth Sciences of the University of Milan for her assistance in collecting XRD spectra, Dr. Eleonora Giulia Terruzzi for collecting part of the experimental data, Dr. Norberto Chiodini from University of Milano-Bicocca for his assistance in collecting LA-ICP

data, and Dr. Bruno Vodopivec from the “Piattaforma di Microscopia—University of Milano-Bicocca” for his assistance in collecting SEM images.

Author contributions Conceptualization: RL, AZ, and IA; methodology and investigation: RL, AZ, VG, and IA; formal analysis: RL; writing—original draft preparation: RL and IA; writing—review and editing: all the authors; supervision: RL, AP, and LP; resources: LP. All the authors read and approved the final manuscript.

Funding Open access funding provided by Università degli Studi di Milano - Bicocca within the CRUI-CARE Agreement.

Declarations

Conflict of interests The authors have no relevant financial or non-financial interests to disclose. The authors declare no competing interests.

Open Access This article is licensed under a Creative Commons Attribution 4.0 International License, which permits use, sharing, adaptation, distribution and reproduction in any medium or format, as long as you give appropriate credit to the original author(s) and the source, provide a link to the Creative Commons licence, and indicate if changes were made. The images or other third party material in this article are included in the article's Creative Commons licence, unless indicated otherwise in a credit line to the material. If material is not included in the article's Creative Commons licence and your intended use is not permitted by statutory regulation or exceeds the permitted use, you will need to obtain permission directly from the copyright holder. To view a copy of this licence, visit <http://creativecommons.org/licenses/by/4.0/>.

References

- Apetz R, Van Bruggen MP (2003) Transparent alumina: a light-scattering model. *J Am Ceram Soc* 86:480–486. <https://doi.org/10.1111/j.1151-2916.2003.tb03325.x>
- Bappu M (1952) Spectroscopic study of amethyst quartz in the visible region. *Indian J Phys* 26(1):1–14
- Barry TI, McNamara P, Moore WJ (1965) Paramagnetic resonance and optical properties of amethyst. *J Chem Phys* 42:2599–2606. <https://doi.org/10.1063/1.1696338>
- Başbüyük Z (2018) Mineralogical, geochemical, and gemological characteristics of silicic gemstone in Aydınçık (Yozgat-Turkey). *Arab J Geosci* 11:292. <https://doi.org/10.1007/s12517-018-3615-2>
- Büyükonak G (1985) Distribution of the major and trace elements in the volcanic rocks of Yozgat area Turkey. *Bull Miner Res Explor Inst of Turkey* 105–106:4
- Cheng R, Guo Y (2020) Study on the effect of heat treatment on amethyst color and the cause of coloration. *Sci Rep* 10:1–12. <https://doi.org/10.1038/s41598-020-71786-1>
- Czaja M, Kaździółka-Gaweł M, Konefał A, Sitko R, Teper E, Mazurak Z, Sachanbiński M (2017) The Mössbauer spectra of prasiolite and amethyst crystals from Poland. *Phys Chem Miner* 44:365–375. <https://doi.org/10.1007/s00269-016-0864-z>
- Deer WA, Howie RA, Wise WS, Zussman J (2004) Rock-forming minerals. Framework silicates: silica minerals, feldspathoides and the zeolites, vol 4B. Geological Society, Bath
- Dennen WH, Puckett AM (1972) On the chemistry and color of amethyst. *Can Miner* 11:448–456
- Dumańska-Słowik M, Powolny T, Sikorska-Jaworowska M, Gaweł A, Kogut L, Poloński K (2018) Characteristics and origin of agates from Płóczki Górne (Lower Silesia, Poland): a combined microscopic, micro-Raman, and cathodoluminescence study. *Spectrochim Acta A Mol Biomol Spectrosc* 192:6–15. <https://doi.org/10.1016/j.saa.2017.11.005>
- Di Benedetto F et al (2010) A Fe K-Edge XAS study of amethyst. *Phys Chem Miner* 37:283–289. <https://doi.org/10.1007/s00269-009-0332-0>
- Flörke O, Köhler-Herbertz B, Langer K, Tönges I (1982) Water in microcrystalline quartz of volcanic origin: agates. *Contrib Miner Petrol* 80:324–333. <https://doi.org/10.1007/BF00378005>
- Gliozzo E (2019) Variations on the Silica Theme: Classification and Provenance from Pliny to Current Supplies. *EMU Notes Miner* 2:13–85. <https://doi.org/10.1180/EMU-notes.20.2>
- Götze J, Nasdala L, Kleeberg R, Wenzel M (1998) Occurrence and distribution of “moganite” in agate/chalcedony: a combined micro-Raman Rietveld, and cathodoluminescence Study. *Contributions Miner Petrol* 133:96–105. <https://doi.org/10.1007/s004100050440>
- Götze J, Tichomirowa M, Fuchs H, Pilot J, Sharp Z (2001) Geochemistry of agates: a trace element and stable isotope study. *Chem Geol* 175:523–541. [https://doi.org/10.1016/S0009-2541\(00\)00356-9](https://doi.org/10.1016/S0009-2541(00)00356-9)
- Götze J, Möckel R, Pan Y (2020) Mineralogy, geochemistry and genesis of agate—a review. *Minerals* 10:1037. <https://doi.org/10.3390/min10111037>
- Götze J, Pan Y, Müller A (2021) Mineralogy and mineral chemistry of quartz: a review. *Miner Mag* 85:639–664. <https://doi.org/10.1180/mgm.2021.72>
- Graetsch H, Flörke O, Miede G (1987) Structural defects in microcrystalline silica. *Phys Chem Miner* 14:249–257. <https://doi.org/10.1007/BF00307990>
- Hassan F, Cohen AJ (1974) Biaxial color centers in Amethyst Quartz. *Am Miner J Earth Planet Mater* 59:709–718
- Hatipoğlu M, Chamberlain S (2009) Ancient deposit of blue chalcedony in Turkey. *Aust Gemmol* 23:566–573
- Hatipoğlu M, Chamberlain SC, Kibici Y (2013) Characterization of the Sündikendağı deposit of moganite-rich, blue chalcedony nodules, Mayıslar-Sarıcakaya (Eskişehir). *Turkey Ore Geol Rev* 54:127–137. <https://doi.org/10.1016/j.oregeorev.2013.03.004>
- Heaney PJ, Post JE (1992) The widespread distribution of a novel silica polymorph in microcrystalline quartz varieties. *Science* 255:441–443. <https://doi.org/10.1126/science.255.5043.441>
- Heaney PJ, McKeown DA, Post JE (2007) Anomalous behavior at the I 2/a to Imab phase transition in SiO₂-moganite: an analysis using hard-mode Raman spectroscopy. *Am Miner* 92:631–639. <https://doi.org/10.2138/am.2007.2184>
- Kingma KJ, Hemley RJ (1994) Raman spectroscopic study of microcrystalline silica. *Am Miner* 79:269–273
- Lee S, Xu H, Xu H, Neuefeind J (2021) Crystal structure of moganite and its anisotropic atomic displacement parameters determined by synchrotron X-Ray diffraction and X-Ray/neutron pair distribution function analyses. *Minerals* 11:272. <https://doi.org/10.3390/min11030272>
- Masso JD, She C, Edwards DF (1970) Effects of inherent electric and anisotropic forces on Raman spectra in α -Quartz. *Phys Rev B* 1:4179. <https://doi.org/10.1103/PhysRevB.1.4179>
- McMillan PF, Hess AC (1990) Ab initio valence force field calculations for Quartz. *Phys Chem Miner* 17:97–107. <https://doi.org/10.1007/BF00199660>
- Miede G, Graetsch H (1992) Crystal structure of moganite: a new structure type for silica. *Eur J Mineral* 4:693–706. <https://doi.org/10.1127/ejm/4/4/0693>
- Moxon T, Ríos S (2004) Moganite and water content as a function of age in agate: an XRD and thermogravimetric study. *Eur J Mineral* 16:269–278. <https://doi.org/10.1127/0935-1221/2004/0016-0269>

- Murphy RJ (2015) Evaluating simple proxy measures for estimating depth of the ~ 1900 nm water absorption feature from hyperspectral data acquired under natural illumination. *Remote Sens Environ* 166:22–33. <https://doi.org/10.1016/j.rse.2015.05.029>
- Naus H, Ubachs W (2000) Experimental verification of Rayleigh scattering cross sections. *Opt Lett* 25:347–349. <https://doi.org/10.1364/OL.25.000347>
- O'Donoghue M (2006) *Gems: their sources, descriptions and identification*. Butterworth-Heinemann, Oxford
- Park C-S, Shin HS, Yi K, Cho H, Kim Y (2015) Quantitative mapping of trace elements in agate using LA-ICP-MS. *J Analytical Sci Technol* 6:1–8. <https://doi.org/10.1186/s40543-015-0078-x>
- Rodgers K, Cressey G (2001) The occurrence, detection and significance of moganite (SiO₂) among some silica sinters. *Miner Mag* 65:157–167. <https://doi.org/10.1180/002646101550181>
- Rossmann GR (2018) *Colored varieties of the silica minerals Silica*. De Gruyter, Berlin
- Schmidt P, Bellot-Gurlet L, Slodczyk A, Fröhlich F (2012) A hitherto unrecognised band in the Raman spectra of silica rocks: influence of hydroxylated Si–O bonds (silanole) on the Raman moganite band in chalcedony and flint (SiO₂). *Phys Chem Miner* 39:455–464. <https://doi.org/10.1007/s00269-012-0499-7>
- Schmidt P, Bellot-Gurlet L, Léa V, Sciau P (2013) Moganite detection in silica rocks using Raman and infrared spectroscopy. *Eur J Mineral* 25:797–805. <https://doi.org/10.1127/0935-1221/2013/0025-2274>
- Seifert W, Rhede D, Thomas R, Förster H-J, Lucassen F, Dulski P, Wirth R (2011) Distinctive properties of rock-forming blue quartz: inferences from a multi-analytical study of submicron mineral inclusions. *Miner Mag* 75:2519–2534. <https://doi.org/10.1180/minmag.2011.075.4.2519>
- Smith DK (1998) Opal, cristobalite, and tridymite: noncrystallinity versus crystallinity, nomenclature of the silica minerals and bibliography. *Powder Diffr* 13:2–19. <https://doi.org/10.1017/S0885715600009696>
- Umari P, Pasquarello A, Dal Corso A (2001) Raman scattering intensities in α -Quartz: a first-principles investigation. *Phys Rev B* 63:094305. <https://doi.org/10.1103/PhysRevB.63.094305>
- Walger E, Mattheß G, Seckendorff V, Liebau F (2009) The formation of agate structures: models for silica transport, agate layer accretion, and for flow patterns and flow regimes in infiltration channels. *Neues Jahrbuch Für Mineralogie-Abhandlungen* 186:113–152. <https://doi.org/10.1127/0077-7757/2009/0141>
- Zhang X, Ji L, He X (2020) Gemological characteristics and origin of the Zhanguohong agate from Beipiao Liaoning Province, China: a combined microscopic, X-Ray diffraction, and Raman spectroscopic study. *Minerals* 10:401. <https://doi.org/10.3390/min10050401>
- Zolensky ME, Sylvester PJ, Paces JB (1988) Origin and significance of blue coloration in quartz from Llano Rhyolite (llanite), north-central Llano County, Texas. *Am Miner* 73:313–323

Publisher's Note Springer Nature remains neutral with regard to jurisdictional claims in published maps and institutional affiliations.